Non-intrusive, *in situ* detection of ammonia in hot gas flows with mid-infrared degenerate four-wave mixing at 2.3 μm

A.-L. Sahlberg,* D. Hot, M. Aldén and Z. S. Li

Abstract

We demonstrate non-intrusive, *in situ* detection of ammonia (NH_3) in reactive hot gas flows at atmospheric pressure using mid-infrared degenerate four-wave mixing (IR-DFWM). IR-DFWM excitation scans were performed in the $\nu_2+\nu_3$ and $\nu_1+\nu_2$ vibrational bands of NH_3 around 2.3 μm for gas flow temperatures of 296, 550 and 820 K. Simulations based on spectroscopic parameters from the HITRAN database have been compared with the measurements in order to identify the spectral lines, and an absorption spectrum at 296 K has also been measured to compare with the IR-DFWM spectra. The signal-to-noise ratio of the IR-DFWM measurement was found to be higher than that of the absorption measurement. Some spectral lines in the measured IR-DFWM and absorption spectra had no matching lines in the HITRAN simulation. The detection limit of NH_3 diluted in N_2 with IR-DFWM in this spectral range was estimated at 296, 550 and 820 K to be 1.36, 4.87 and 7.06×10^{16} molecules/cm^3. The dependence of the NH_3 IR-DFWM signal on the quenching properties of the buffer gas flow was investigated by comparing the signals for gas flows of N_2, Ar and CO_2 with small admixtures of NH_3. It was found that the signal dependence on buffer gas was large at room temperature but decreased at elevated temperatures. These results show the potential of IR-DFWM for detection of NH_3 in combustion environments.

Keywords: Mid-infrared, degenerate four-wave mixing, ammonia

Introduction

Ammonia (NH_3) is a key species for the fertilizer industry and for catalytic and non-catalytic reduction of nitric oxides (NO_x) in combustion processes.[1] In recent years, biomass has gained much interest as a renewable alternative to fossil fuels.[2,3] NH_3 is often generated during biomass pyrolysis and gasification.[4,5] The widespread use and occurrence of NH_3 in combination with its toxicity and corrosive nature introduces the need of NH_3 detection and monitoring.

Laser-based diagnostic techniques enable non-invasive *in situ* measurements of combustion-relevant parameters.[6] The increasing role of NH_3 in biomass combustion means it is of high interest to develop techniques for detection of NH_3 in combustion situations. The electronic resonances for NH_3 are located in the vacuum-ultraviolet, making it difficult to measure NH_3 using conventional laser techniques.[7] Photofragmentation of NH_3 and subsequent NH fluorescence detection has been applied as a means to circumvent this problem.[8] Another option is to probe the electronic resonances using two-photon processes, which has been demonstrated with laser-induced fluorescence,[9,10] polarization spectroscopy[11] and four-wave mixing techniques.[12,13] NH_3 has also been detected by probing ro-vibrational resonances in the infrared. Previous laser measurements of NH_3 have been achieved using line-of-sight absorption techniques around 10 μm.[14,15] Highly sensitive NH_3 detection around 1.5 μm has been demonstrated using diode-laser absorption spectroscopy[16] and fiber laser intracavity absorption

spectroscopy.[17] Laser-induced grating spectroscopy for detection of NH_3 has been demonstrated using CO_2 lasers around 10 μm.[18]

Degenerate four-wave mixing (DFWM) is a sensitive, non-intrusive and coherent laser technique that has been widely applied to combustion situations with wavelengths in the ultraviolet (UV)/visible region.[6,19-21] An analytical expression for the DFWM signal was first derived by Abrams and Lind in 1978.[22,23] Since then, the theory and application of DFWM for detection of trace species has been widely studied,[19,24,25] and the results have been reviewed by Kiefer and Ewart.[26]

Recently, mid-infrared DFWM (IR-DFWM) has emerged as a sensitive laser technique for detection of infrared active molecules and radicals that lack easily accessible transitions. Compared to the UV/visible spectral region, few DFWM measurements have been performed with mid-infrared lasers, due to relatively low availability of high power lasers and sensitive, low noise detectors. Detection of e.g. HF,[27] NO_2,[28] jet-cooled C_2H_2[29] and CH_4[30] with IR-DFWM has been demonstrated. Sun *et al.* have designed a stable alignment of IR-DFWM in the forward phase-matching geometry and demonstrated the setup for detection of HCl and C_2H_2[31] and for measurements of flame temperatures using H_2O line intensity ratio.[32] Sahlberg *et al.* recently demonstrated detection of CH_3Cl with IR-DFWM[33] using a similar setup. Högstedt *et al.* have demonstrated the use of a novel, low noise upconversion detector for sensitive IR-DFWM measurements of C_2H_2.[34]

The purpose of this paper is to investigate the potential of IR-DFWM as a tool for non-intrusive, *in situ* spatially resolved detection of NH_3 by probing the $\nu_2+\nu_3$ and $\nu_1+\nu_2$ vibrational bands around 4500 cm^{-1} for applications to biomass combustion. For this purpose, the IR-DFWM spectrum of NH_3 diluted in atmospheric gas flows was measured at 296, 550 and 820 K, to determine how the spectral structure and the detection limit change with temperature. The measurements indicate the possibility of IR-DFWM as a sensitive tool both for combustion diagnostics and for spectroscopic investigations in the mid-infrared spectral region.

Experiment

A schematic of the experimental setup is shown in Fig. 1. The laser system has been described in more detail elsewhere[35] and thus only a brief description is provided here. The infrared laser light was provided by a laser system consisting of an injection-seeded Nd:YAG laser (Spectra Physics, PRO 290-10), a dye laser (Sirah, PRSC-D-18) and a frequency mixing unit. The dye laser was pumped by the frequency doubled output (532 nm) of the Nd:YAG laser and the tunable dye laser output around 722 nm was frequency mixed in an $LiNbO_3$ crystal with part of the residual 1064 nm output from the Nd:YAG laser, resulting in mid-infrared laser pulses. This laser beam was further amplified in a second $LiNbO_3$ crystal pumped with another part of the residual 1064 nm beam. The crystals were angle-adjusted to optimize the conversion efficiency during the dye laser wide-range wavenumber scans. The final tunable mid-infrared laser light had a pulse energy around 5 mJ and a pulse duration of 3-4 ns. The wavenumber during the scan is measured in the dye laser control program, and the wavenumber accuracy of our scans was estimated to be ±0.1 cm^{-1}. The line width of the final IR laser output has been measured to be 0.025 cm^{-1}.[36] The IR laser beam was guided through a telescope arrangement (L1, L2) to obtain

a beam size of approximately 2 mm. A CaF_2 window (BS) was placed in the beam path, where the reflection was sent to a power meter in order to monitor the laser power.

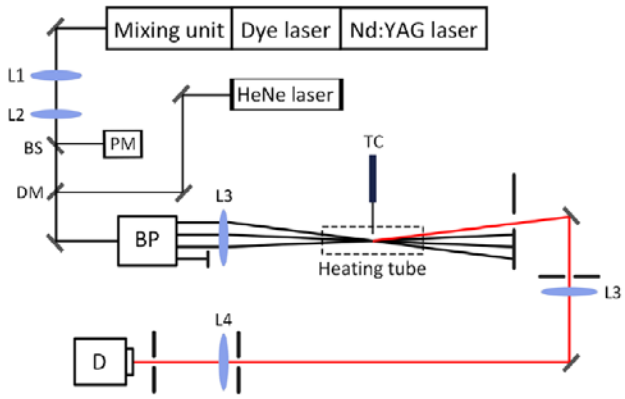

Figure 1. Schematic view of the experimental setup. BP, BOXCARS plates; D, InSb detector; TC, thermocouple; PM, power metre; BS, beam splitter; DM, dichroic mirror; L1, CaF_2 lens, f = 500 mm; L2, CaF_2 lens, f =-200 mm; L3, CaF_2 lens, f = 300 mm; L4, CaF_2 lens, f = 100 mm.

The infrared laser beam was overlapped with a He-Ne laser beam (DM) to facilitate the optical alignment. The laser beam was split into four parallel beams using a set of specially coated BOXCARS plates (BP). A detailed description of the BOXCARS plates can be found elsewhere.[31] Three of these beams were focused by an f = 300 mm CaF_2 lens (L3) into the probe volume in the middle of the gas tube, where the IR-DFWM signal was generated along the pathway of the fourth beam. The pulse energy of each beam was ~1 mJ, which corresponds to ~1.2 MW/mm^2 in the probe volume with the current setup. The IR-DFWM signal beam was collimated by another f = 300 mm CaF_2 lens (L3) and spatially filtered and focused (L4) onto an InSb liquid nitrogen cooled infrared detector (D, Judson technologies, J10D-M204-R04M-60). The probe volume was estimated to be 0.4×0.4×6 mm^3. The IR-DFWM spectrum was obtained by tuning the dye laser wavelength and hence, scanning the IR laser wavelength over the NH_3 absorption lines. The spectra were recorded without accumulation of the data points.

A continuous gas flow consisting of a buffer gas (N_2, Ar or CO_2) with small admixtures of NH_3 was flowed through an open T-shaped heating gas tube, which has been described in a previous work.[33] The tube is made of fused silica which is surrounded by an electrical heating wire and insulation. A thermocouple was inserted through the top of the gas tube in order to measure the gas temperature close to the probe volume. The temperature in the probe volume was assumed to be uniform and the same as what the thermocouple measured. Variable NH_3 concentrations in the gas flow were achieved by adjusting the relative flows of buffer gas and NH_3 using Bronkhorst mass flow controllers. The total gas flow through the tube was ~2-5 liters/min.

An absorption measurement of NH_3 was conducted in a 50-cm long gas cell with CaF_2 windows mounted at the Brewster angle at both ends of the gas cell. A continuous flow, consisting of 2 % NH_3 diluted in N_2, passed through the gas cell at 296 K and atmospheric pressure. The IR laser output was split into two laser beams where one beam was sent through the gas cell and the other was sent through open air, and each of the beams was then directed to an InSb liquid nitrogen cooled detector. The absorption was obtained from the ratio of the signal from the two detectors.

Several neutral density filters were used to reduce the laser energy in order to avoid saturation effects in the measured absorption spectrum.

NH_3 mid-infrared spectral bands and water interference

NH_3 is an oblate symmetric top molecule. In the mid-infrared spectral region, NH_3 has several relatively strong spectral lines belonging to fundamental as well as combination and overtone vibrational bands. Figure 2 shows the line strengths of NH_3 absorption lines in the spectral region 3000-5300 cm^{-1}. The line intensities are taken from the HITRAN database.[37] The lines around 3400 cm^{-1} belong to the v_1, v_3 and $2v_4$ bands, the lines around 5000 cm^{-1} belong to the v_1+v_4 and v_3+v_4 combination bands, and the lines around 4500 cm^{-1} belong to the v_2+v_3 and v_1+v_2 combination bands. The line strengths of the NH_3 transitions in the entire spectral region displayed in Fig. 2 are rather similar. The present investigation employs the v_2+v_3 and v_1+v_2 bands around 4500 cm^{-1}. The rotational levels in the v_2+v_3 and v_1+v_2 bands are described using the quantum numbers J and K, and s or a indicating the inversion symmetry. For example, the line notation ${}^{R}R_3(4)s$ indicates a transition with ΔK=1, ΔJ=1, $K"$=3 and $J"$=4, with inversion symmetry s.

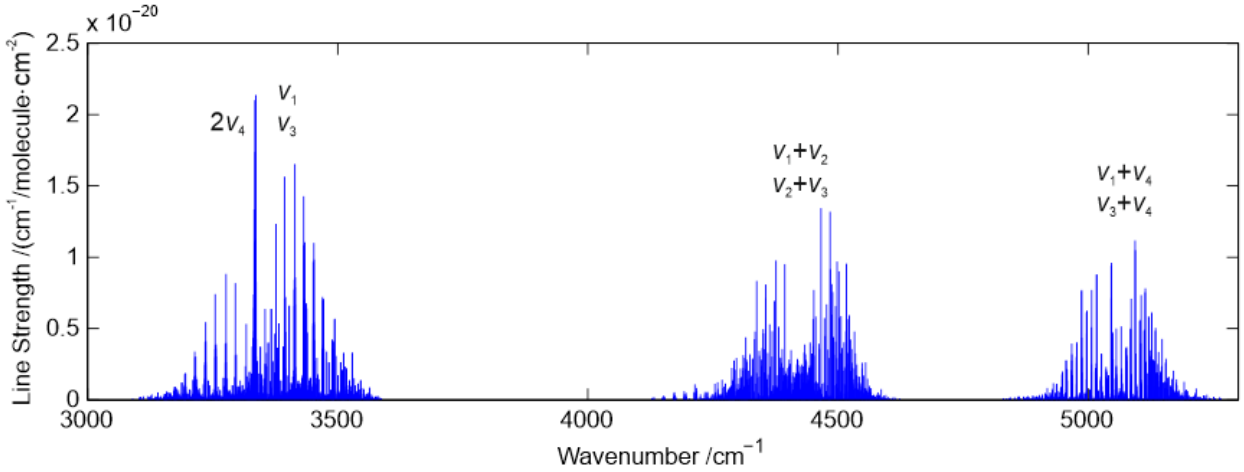

Figure 2. The HITRAN line strengths of NH_3 transitions at 296 K in the mid-infrared spectral region. Assignments for the different bands are included in the figure.

Water has strong absorption lines in the mid-infrared spectral region, so any application of IR spectroscopy in combustion situations needs to consider the interference from H_2O spectral lines at flame temperatures. Figure 3 shows the line strengths of water lines at 296 K and 1500 K, taken from the HITRAN[37] and HITEMP[38] databases. It is clear that a great advantage of NH_3 detection in the v_2+v_3 and v_1+v_2 bands is that in this case the interference from H_2O spectral lines is much weaker than in the other bands shown in Fig. 2, both at room temperature and at flame temperatures.

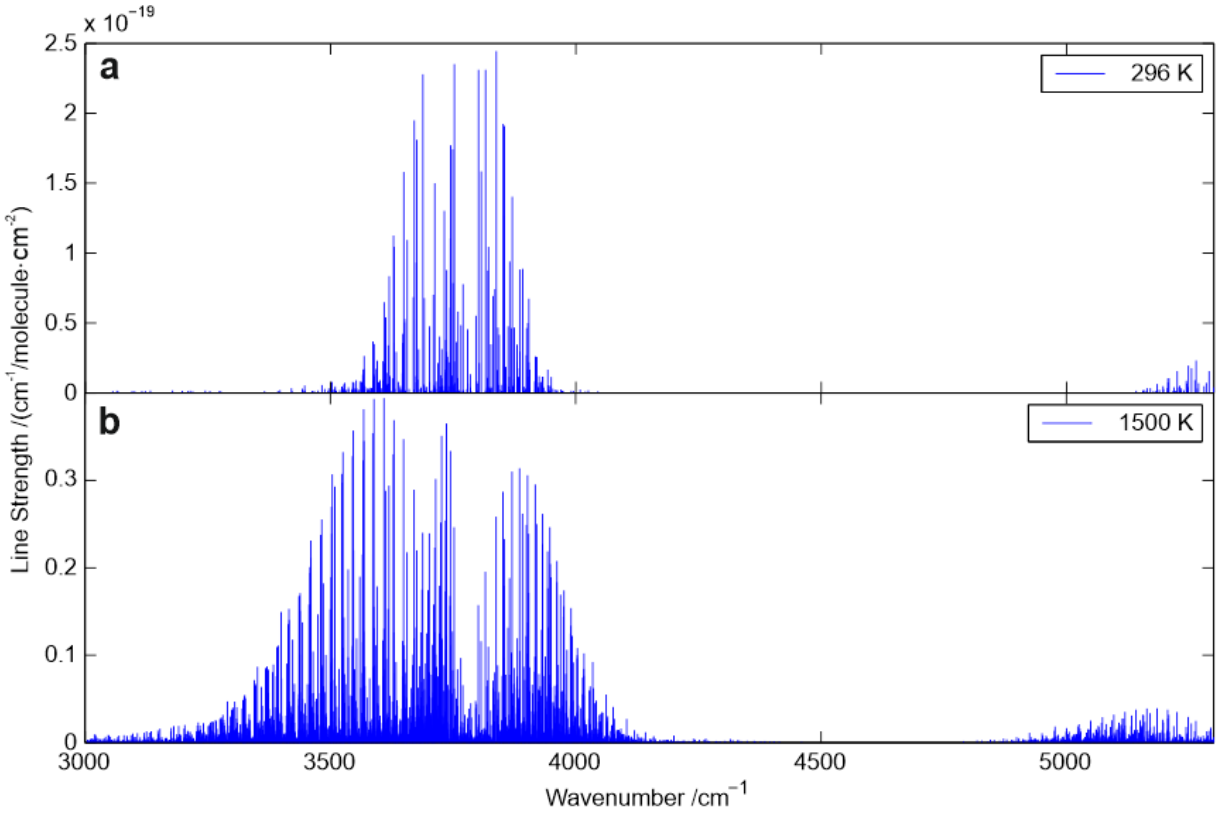

Figure 3. The line strengths of H_2O transitions from the HITRAN and HITEMP databases at (a) 296 K and (b) 1500 K.

Results and Discussion

The graphs in Fig. 4 show a comparison of the measured and simulated IR-DFWM and absorption spectra of the $\nu_2+\nu_3$ and $\nu_1+\nu_2$ bands of NH_3. Figure 4a shows the measured absorption spectrum of 2 % NH_3 diluted in N_2 over a path length of 50 cm. The red curve shows a simulated absorption spectrum, calculated using the Beer-Lambert law

$$A = 1 - e^{-\sigma(\nu)NL} \tag{1}$$

where N is the number density and L is the absorption path length. The absorption cross section σ as a function of wavenumber ν was calculated using the following relation

$$\sigma(\nu) = \sum_i S_i g(\nu) \tag{2}$$

where S_i is the line strength taken from the HITRAN database and $g(\nu)$ is the line shape function, which was approximated by a Lorentzian function with a line width given by the collision line width specified in the HITRAN database.

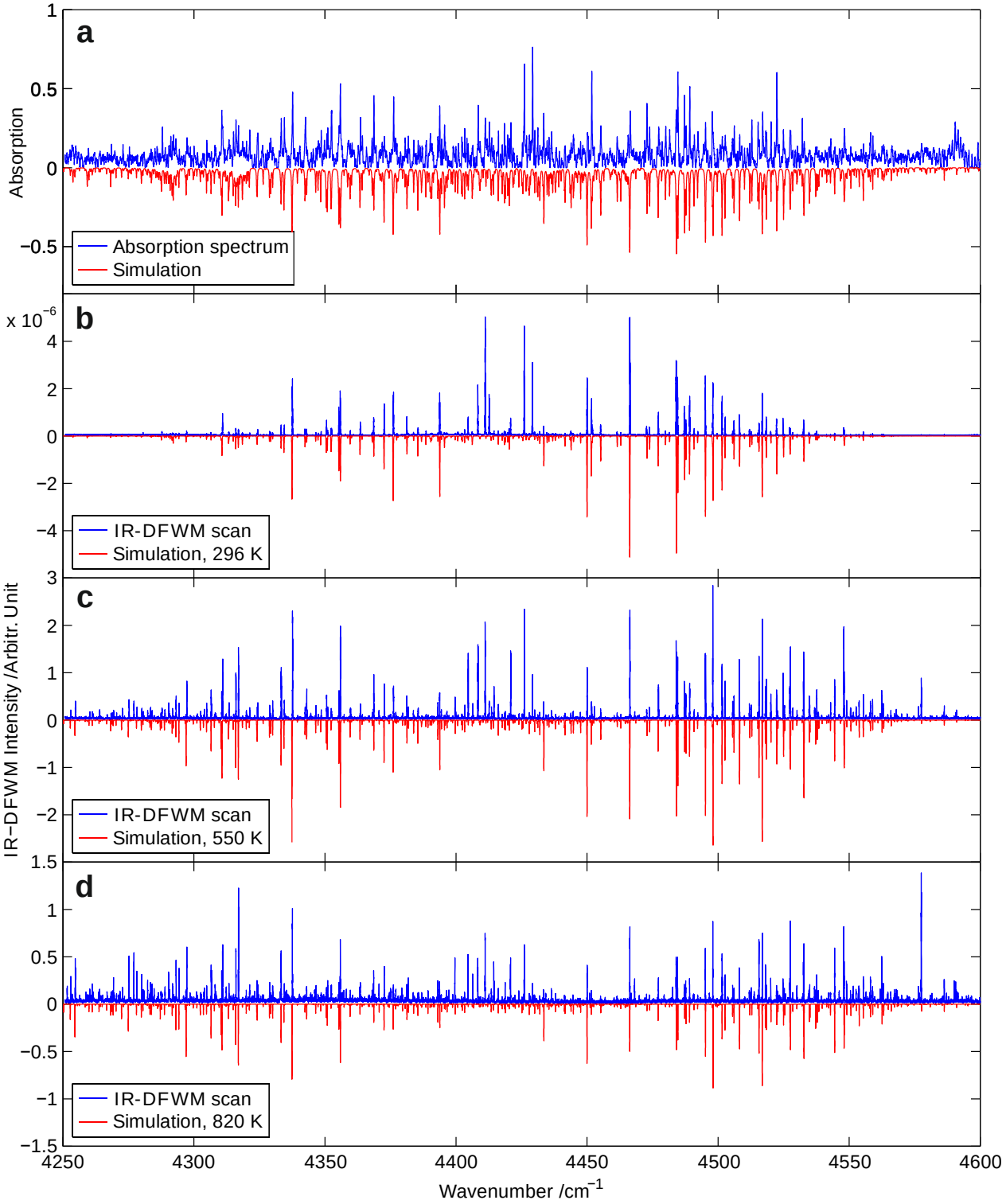

Figure 4. A comparison of the measured (blue) and simulated (red) (a) absorption spectrum of NH3 at 296 K for an NH_3 concentration of 2% and a path length of 50 cm, (b) mid-infrared degenerate four-wave mixing (IR-DFWM) spectrum at 296 K, 0.99% NH_3 (c) IR-DFWM spectrum at 550 K, 1.97% NH_3 and (d) IR-DFWM spectrum at 820 K, 2.93% NH_3. The intensities of the simulated IR-DFWM spectra were adjusted to the best fit to the measurements.

The recorded absorption spectrum compares quite well with the simulation over most of the spectrum. As a linear technique, the absorption spectrum is easy to simulate and it is straightforward to relate the recorded absorption to species concentration. It is valuable to have a recorded absorption spectrum to compare with the IR-DFWM measurements, as the latter is sometimes more difficult to simulate for complicated molecular spectra.[33] Note that pulsed lasers are generally not optimal for absorption measurements, due to laser energy shot-to-shot fluctuations which complicates the data analysis. For example, the broad structure around 4590 cm^{-1} in the measured absorption spectrum, which does not have a match in the simulation, probably originates from background noise due to laser fluctuations.

Figures 4b-d show the measured IR-DFWM spectra of NH_3 diluted in N_2 at 296, 550 and 820 K, compared with simulations of the IR-DFWM signal at the same temperatures. The DFWM signal for saturating laser intensities was simulated using the empirical relation[33]

$$I_{DFWM} \propto N^2 \sigma(\nu)^2 \tag{3}$$

where N is the number density of the gas. The relation for saturating DFWM was used in the simulations since this gave the best agreement with the experiment. The absorption cross section $\sigma(\nu)$ was calculated as shown in Eq. 2, but the line shape function $g(\nu)$ was approximated by a Voigt profile, with parameters chosen to match the measured line shapes at each temperature. In the figures, the simulation from Eq. 3 was multiplied with a calibration constant to achieve the best fit to the measured line intensities. Line notations for selected lines in the spectra are included in Supplementary Information, along with text files containing the raw data for the spectra.

Comparing the absorption and IR-DFWM spectra at 296 K in Fig. 4 a-b, it is clear that the IR-DFWM spectrum has better sensitivity and higher signal-to-noise ratio than the absorption spectrum. The strong lines in the center of the spectral range are enhanced in IR-DFWM while the weak lines located in the wings of spectrum appear even weaker because of the quadratic dependency on σ. For the most part, the measured IR-DFWM spectra in Fig. 4b-d agree quite well with the simulations. Small deviations of the measured and simulated line intensity for individual lines are likely to be caused by the unstable mode structure of the laser, which can cause fluctuations in the signals.[39,40] However, there are larger differences which cannot be explained by noise in the signals. At all three temperatures, the measured spectra in the interval 4390-4400 cm^{-1} show several strong lines without corresponding lines in the simulation. Also, at 550 and 820 K in Fig. 4c-d, there is an unforeseen strong spectral line at about 4577.5 cm^{-1}. In the following sections, this will be discussed in more detail.

4390-4440 cm^{-1}

Figure 5 shows the measured IR-DFWM spectrum at 296 K in the interval 4390-4440 cm^{-1}. There are six relatively strong spectral lines (numbered 1-6 in the figure) which do not match any transition in the simulation. The lines are present at all temperatures and are much stronger than any of the lines in the simulation. Figure 6 shows the measured and simulated absorption

spectrum in the same interval. The six lines mentioned above are present in both experimental spectra, absorption and IR-DFWM. Careful examination of the IR-DFWM and the absorption spectra and comparison with the HITRAN data shows that all the HITRAN weak transitions are present as separate signals around the extra lines, and thus cannot be responsible for these signals.

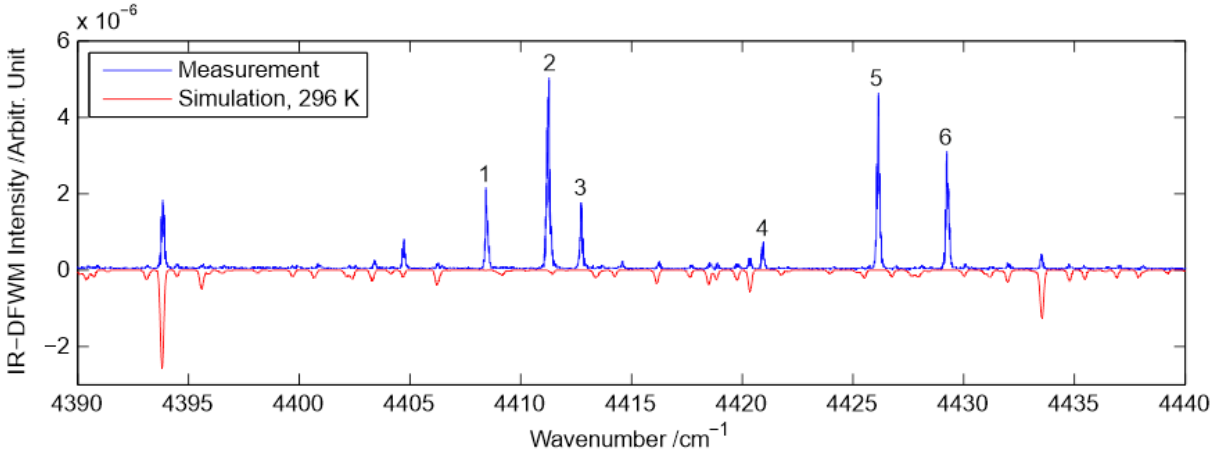

Figure 5. A comparison of the measured (blue) and simulated (red) mid-infrared degenerate four-wave mixing (IR-DFWM) spectrum at 296 K in the interval 4390–4440 cm^{-1}. The numbers 1–6 indicate six strong spectral lines without corresponding lines in the simulation. The intensities of the simulated spectra were adjusted to the best fit to the measurements.

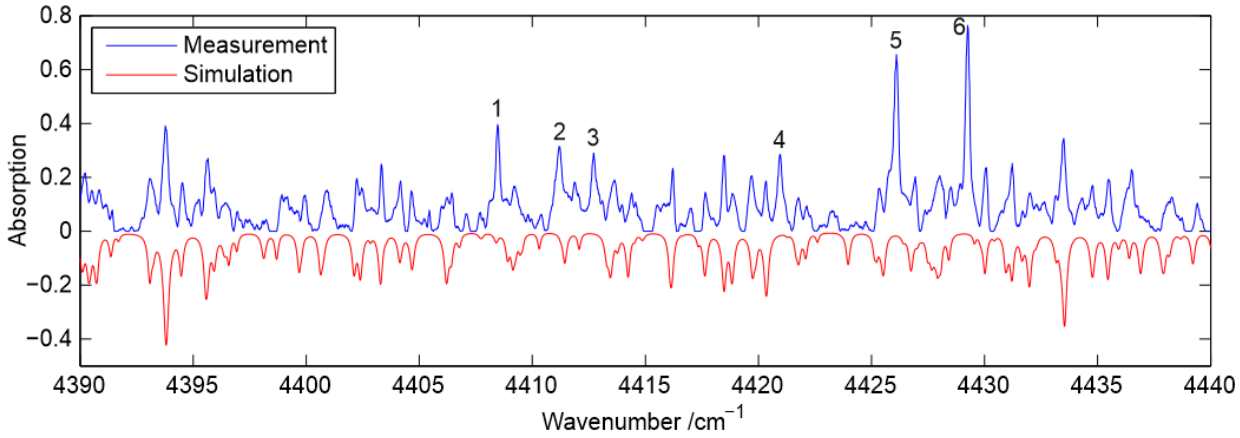

Figure 6. A comparison of the measured (blue) and simulated (red) absorption spectrum at 296 K in the interval 4390–4440 cm^{-1}. The numbers 1–6 indicate the six spectral lines without corresponding lines in the simulation.

The first high-resolution study of the ν_2+ν_3 and ν_1+ν_2 bands of NH_3 was performed in 1958 by Benedict *et al.*[41], using a 15,000 lines-per-inch grating spectrometer with a resolution of 0.08 cm^{-1}. They observed a large number of spectral lines in this spectral region and managed to assign these lines to transitions within the ν_2+ν_3 and ν_1+ν_2 bands. The extra lines 1-6 observed in Fig. 5 are also present in the spectra they published, and surrounded by transitions that match the HITRAN database and our measurements. Lines 1-3 were identified as the $^{R}Q_0(5)s$, $^{R}Q_0(3)s$ and $^{R}Q_0(1)s$ lines of the ν_2 + ν_3 band, while lines 4-6 were shown in the spectra but not assigned. The

fact that the extra lines have been observed before supports our conclusion that these are NH_3 lines, and not lines from any contaminant species present in our setup.

The data for NH_3 in the HITRAN 2012 database[37] is based on an extensive recalculation, performed by Down *et al*.,[42] of the data in the HITRAN 2008 database.[43] They updated the line assignments with a new set of quantum numbers that better described the levels, and changed or removed transitions that were incorrectly labelled. For the v_2+v_3 and v_1+v_2, the changes performed were relatively small. The data for the v_2+v_3 and v_1+v_2 bands in the HITRAN 2008 database originates from high resolution Fourier Transform measurements performed by Urban *et al*.[44] This study identified a large number of transitions from the v_2+v_3 and v_1+v_2 bands in NH_3, but the six extra lines in Fig. 5 and 6 were not mentioned in their analysis. They also assigned some lines to the v_2+2v_4 band, but the analysis was not complete due to the low signal-to-noise ratio for the weaker lines. Insufficient line intensities also made it impossible to make assignment of the lines to the $3v_2+v_4$, $4v_2$ and $5v_2$ bands. Failure to include all transitions in the database could explain why the extra spectral lines in our measurements are not present in the simulation, although it is unlikely that these weak bands are responsible for the strong spectral lines observed in Fig. 5 and 6.

The relative intensity of the lines does not match between the IR-DFWM spectrum and the absorption spectrum. As mentioned before, pulsed lasers are not ideal for absorption measurements. Background noise from the laser energy shot-to-shot fluctuations means it is hard to trust the absolute values of the measured peak absorption. Also, it has been shown before that the IR-DFWM simulation of closely spaced lines is complicated and requires detailed knowledge of the coherent addition of signals belonging to different transitions,[45-47] and that the IR-DFWM intensity does not always match with the absorption intensity of closely spaced transitions.[33] In the measurements by Benedict *et al.*,[41] the absorption strength of all six lines was similar, although their measurements were performed at low pressures, which makes a direct comparison to our measurements difficult.

4480-4520 cm^{-1}

Figure 7 shows the measured IR-DFWM spectrum at 550 K in the spectral region 4480-4520 cm^{-1}. In this spectral range, the agreement between measurement and simulation is relatively good. As mentioned before, any difference between the measured and simulated line intensity is probably due to the unstable mode structure of the IR laser system. This is also why the line shapes of the IR-DFWM spectral lines are not perfect Lorentzian profiles. Any difference between the center wavenumber of the measured and simulated IR-DFWM lines is within the IR laser wavelength precision.

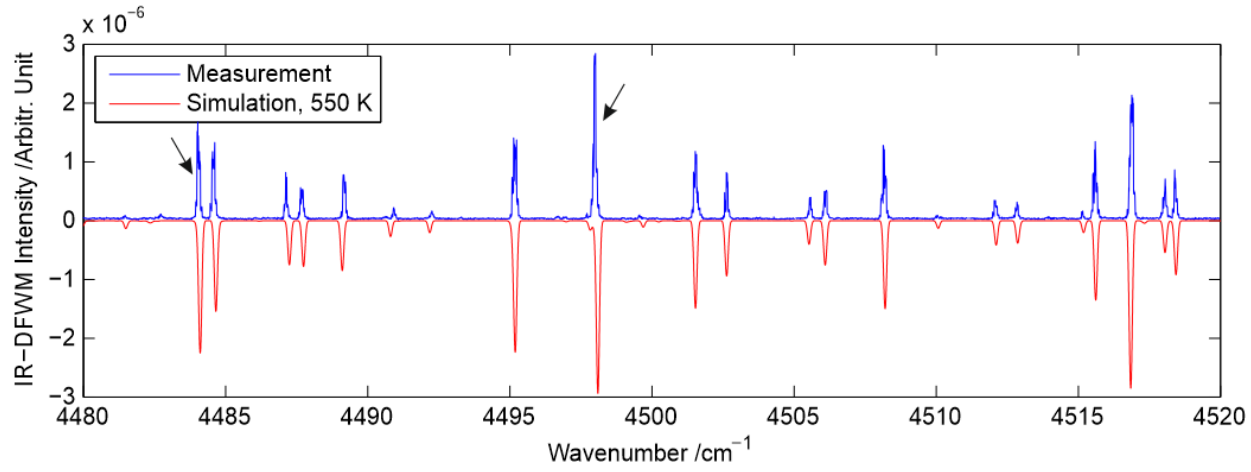

Figure 7. A comparison of the measured (blue) and simulated (red) mid-infrared degenerate four-wave mixing (IR-DFWM) spectrum at 550 K in the interval 4480–4520 cm^{-1}. In this spectral region, the simulation and measurement agree very well at all investigated temperatures. The intensities of the simulated spectra were adjusted to the best fit to the measurements. The arrows indicate the lines used for the detection limit and buffer gas dependence measurements.

4550-4600 cm^{-1}

At 820 K, and to a lesser degree at 550 K, hot lines that were absent at room temperature start to appear in the measured IR-DFWM spectra. Figure 8 shows the spectrum at 820 K in the interval 4550-4600 cm^{-1}. The numbers 1-8 indicate selected lines in the measurement that have no corresponding lines in the simulation. Line number 6 at 4577.5 cm^{-1} is very close to the $^{R}R_6(10)a$ line of the $\nu_2+\nu_3$ band at 4577.66 cm^{-1}, but has a much higher line intensity.

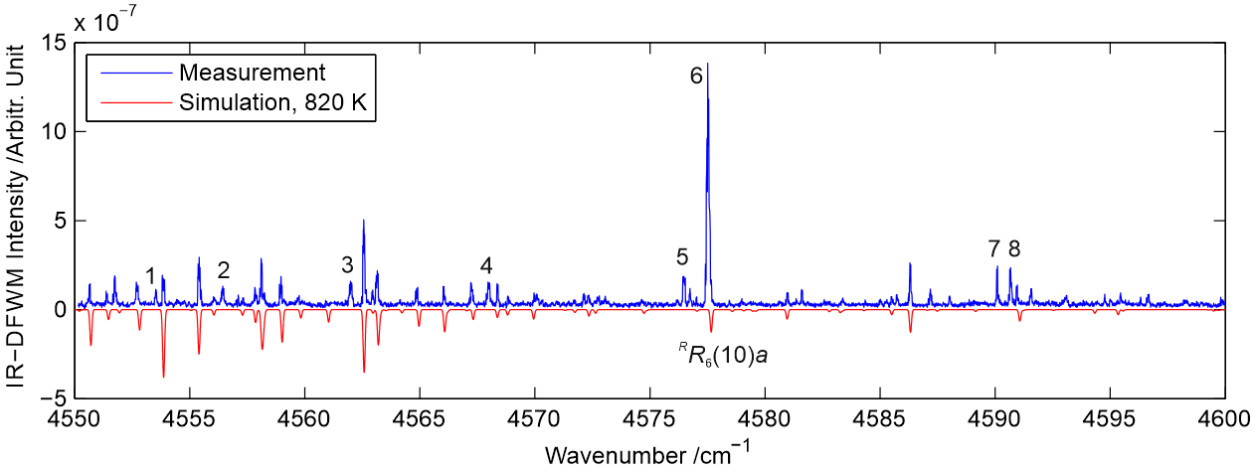

Figure 8. Comparison of the measured (blue) and simulated (red) mid-infrared degenerate four-wave mixing (IR-DFWM) spectrum at 820 K in the interval 4550–4600 cm^{-1}. The numbers 1–8 indicate eight spectral lines that have no corresponding lines in the simulation. The weak simulated line at 4577.66 cm^{-1} is the $^{R}R_6(10)a$ line from the $\nu_2+\nu_3$ band. The intensities of the simulated spectra were adjusted to the best fit to the measurements.

The HITRAN database contains limited information about NH_3 hot bands in this spectral region. Therefore, it is likely that lines 1-8 belong to some hot bands of NH_3 which have too low intensity to be identified in room temperature spectra, but gain intensity as the higher levels get populated at elevated temperatures. The presence of many closely spaced transitions in line 6 could explain why the signal for this line is so strong compared to the other hot lines. It is also possible that the NH_3 is decomposing in the hot environment, and that the extra lines originate from some other species in the flow. However, the hot lines start to appear in the spectrum already at 550 K, at which temperature the decomposition of NH_3 should be completely negligible.[48,49] Even at 820 K, the gas flows used in these experiments are high enough that the pyrolysis can be assumed to be negligible for the time the NH_3 gas spends in the heating tube.

Text files containing the raw data for the IR-DFWM spectra at each temperature are available in Supplementary Information.

NH_3 detection limit

To test the detection limit of these measurements, the IR-DFWM signal dependence on the NH_3 concentration diluted in N_2 gas flows was investigated. Five consecutive IR-DFWM scans were performed over the strongest line in the spectrum for a number of NH_3 concentrations at each temperature. At room temperature the scan was performed over the $^{R}R_3(3)a$ line from the $\nu_2+\nu_3$ band at 4484.1 cm^{-1}. Figure 9 shows the IR-DFWM line-integrated signal intensity as a function of NH_3 concentration at 296 K. The line-integrated signal intensity is defined as the area under the recorded IR-DFWM line. The inset is the IR-DFWM signal for 1151 ppm of NH_3, showing both the $^{R}R_3(3)a$ line and the weaker neighboring $^{R}R_3(4)s$ line at 4484.7 cm^{-1}. At 550 and 820 K, the concentration dependence scan was instead performed over the $^{R}R_6(6)s$ line of the $\nu_2+\nu_3$ band at 4498.1 cm^{-1}. These lines are indicated with arrows in Figure 7. The detection limits at each temperature were estimated by extrapolating the fitted quadratic curve down to a value where the signal-to-noise ratio is 1, and the resulting detection limits are shown in Table 1.

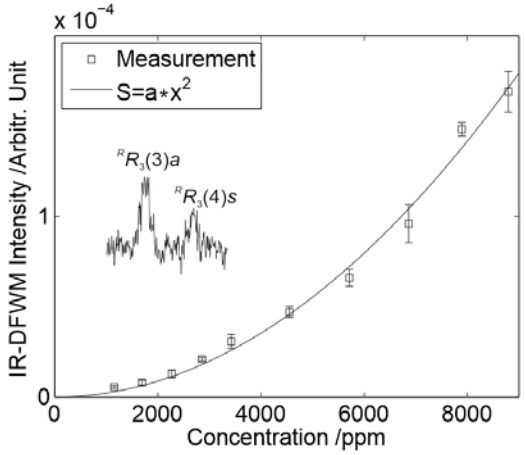

Figure 9. The line integrated mid-infrared degenerate four-wave mixing (IR-DFWM) signal intensity dependence on the concentration of NH_3 diluted in N_2 at 296 K for the $^{R}R_3(3)a$ line from the $\nu_2+\nu_3$ band at 4484.1 cm^{-1}. Each point on the curve is an average of five measurements, and the error bars represent the standard deviation. The inset shows the scan over the $^{R}R_3(3)a$ line and the weaker $^{R}R_3(4)s$ line at 1151 ppm NH_3 concentration.

Buffer gas dependence

The dependence of the IR-DFWM signal on the buffer gas environment was investigated by performing a series of measurements for NH_3 diluted in three different buffer gases (Ar, CO_2 or N_2) at 296, 550 and 820 K. Figure 10 shows the line-integrated IR-DFWM signal intensity of the $^{R}R_3(3)a$ line of the v_2+v_3 band for NH_3 diluted in Ar, CO_2 or N_2. The NH_3 concentration in the gas flows was 0.99, 1.97 and 2.93 % at 296, 550 and 820 K, respectively. The signals are an average of five measurements and the error bars indicate the standard deviation of the five measurements. At each temperature, all three signals are normalized to the signal recorded in Ar. It is clear that the signal is strongly dependent on the buffer gas, but the dependence decreases with increasing temperature. Collisional quenching as well as rotational and vibrational energy transfer contributes to the IR-DFWM dependence on the buffer gas. The dependence decreases at higher temperatures due to lower collision rates. At room temperature, the signal in Ar is ~16 times stronger than the signal in CO_2, while at 820 K the signal in Ar is only ~2.5 times larger than the signal in CO_2. This suggests that collision factors should not have a significant effect on IR-DFWM measurements in atmospheric pressure flames. This is in agreement with previous DFWM measurements in flames, where the derived flame temperatures from OH spectra were found to be almost independent on collisional correction factors.[50]

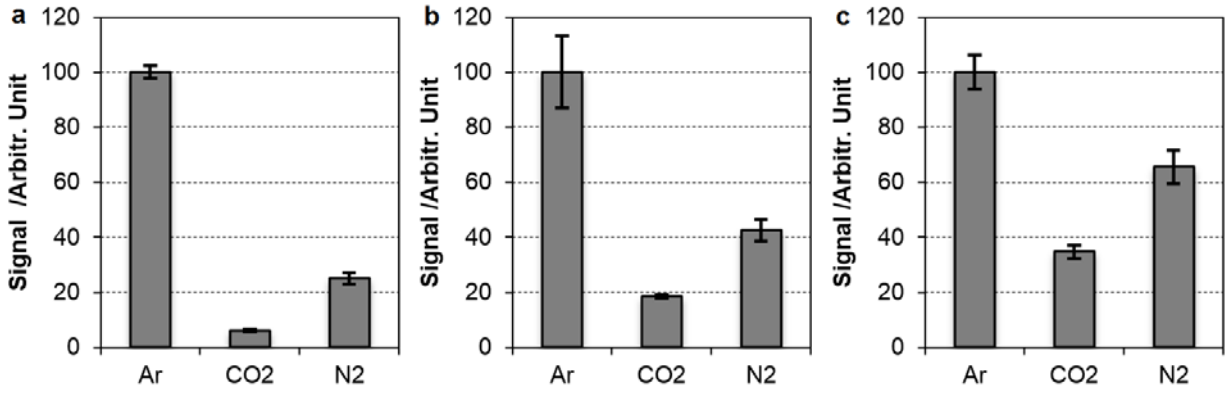

Figure 10. A comparison of the relative mid-infrared degenerate four-wave mixing signal of NH_3 diluted in Ar, CO_2 or N_2, for (a) 296, (b) 550 and (c) 820 K. The signals in each graph are normalised to the signal in the Ar buffer gas. The three plots show the line-integrated signals for an average of five measurements, and the error bars represent the standard deviation of the measurements.

Previous theoretical and experimental studies predict that the DFWM signal for saturating laser intensities should be relatively insensitive to collisional quenching, while unsaturated signals have a stronger pressure dependence.[25,51,52] These theoretical studies assumed non-saturating probe beams and the phase-conjugate geometry. Therefore, the results may not be directly applicable to our measurement situation, where we have equal pump and probe intensities and the forward pump geometry.[53] The recorded IR-DFWM spectra in Fig. 4 are well simulated by a σ^2-dependence, which suggests the laser energies in these experiments were close to saturation.[54] Saturation is more easily achieved at elevated temperatures, which could explain why the collision dependence is smaller at higher temperatures. A detailed study of saturation influence

on collision effects in IR-DFWM is beyond the scope of this work. Further work is required to study this in more detail.

Table 1: The estimated detection limit for NH_3 diluted in N_2 atmospheric pressure gas flows at each temperature.

Temperature /K	Detection limit /ppm	Detection limit /(molecules/cm^3)
296	550	1.4×10^{16}
550	3700	4.9×10^{16}
820	7900	7.1×10^{16}

Summary

We have demonstrated successful detection of NH_3 with IR-DFWM in the v_2+v_3 and v_1+v_2 vibrational bands around 2.3 μm for 296, 550 and 820 K. A comparison between the measured IR-DFWM spectrum of NH_3 and a simulation from the HITRAN database shows a good agreement in line position and intensity for most parts of the spectrum. A large disagreement is found in the interval 4390-4440 cm^{-1}, where there are six relatively strong spectral lines in the measured IR-DFWM spectrum of NH_3 without any match in the simulation. These extra lines were observed in previous measurements of the NH_3 absorption spectrum in this spectral region,[41] but are not included in later studies[42,44] or in the HITRAN database.[37] Further work is required to determine the origin of the discrepancies. At elevated temperatures there is also a strong spectral line at 4577.5 cm^{-1} and several weaker lines without a match in the HITRAN database. To our knowledge, there have been no measurements of the hot NH_3 spectrum in this spectral region before. Therefore, the HITRAN database contains limited information about the hot bands of NH_3. This demonstrates the potential of IR-DFWM as a spectroscopic tool for investigation of mid-IR spectral lines at both room and elevated temperatures.

The IR-DFWM signal intensity at room temperature was found to depend strongly on the buffer gas, being ~16 times higher in Ar compared with CO_2. This dependence decreased at elevated temperatures, and at 820 K the signal in Ar was only ~2.5 times larger than that in CO_2. This seems to indicate that flame measurements of NH_3 with IR-DFWM are rather insensitive to collision factors, which opens the possibility for quantitative concentration measurements.

Detection limits at 296, 550 and 820 K in N_2 gas flows were estimated to be of 1.36, 4.87 and 7.06×10^{16} molecules/cm^3, respectively. These detection limits could be greatly improved by utilizing the more sensitive upconversion detector,[55] which has been demonstrated before to give at least 10 times improvement in detection limit for IR-DFWM measurements.[34] The concentration of NH_3 released during combustion of biomass varies with the fuel.[56] For many applications, the detection limits achieved here should be sufficient for in situ diagnostics in biomass combustion.[56,57] Detection of NH_3 in this spectral region appears to be relatively free from water interference and interference from other species which could be present in biomass combustion environments. These measurements show that IR-DFWM has great potential for sensitive, *in situ* detection of NH_3 in biomass combustion with high spectral resolution.

Text files containing the raw data for the IR-DFWM spectra at each temperature, and line notations for selected spectral lines in the figures, are available in Supplementary Information.

Acknowledgements

This work was financed by the Knut & Alice Wallenberg foundation, STEM (Swedish Energy Agency), ERC (European Research Council) and VR (Swedish Research Council).

References

[1] L. J. Muzio, G. C. Quartucy, *Prog. Energy Combust. Sci.* **1997**; *23*, 233.
[2] M. Parikka, *Biomass Bioenerg.* **2004**; *27*, 613.
[3] M. Balat, *Energy Sources, Part A* **2009**; *31*, 1160.
[4] J. Leppälahti, *Fuel* **1995**; *74*, 1363.
[5] P. Glarborg, A. D. Jensen, J. E. Johnsson, *Prog. Energy Combust. Sci.* **2003**; *29*, 89.
[6] K. Kohse-Höinghaus, *Prog. Energy Combust. Sci.* **1994**; *20*, 203.
[7] C. Bing-Ming, L. Hsiao-Chi, C. Hong-Kai, B. Mohammed, L. Yuan-Pern, M. M. Alexander, L. C. Lee, L. Mao-Chang, L. Y. Yuk, *Astrophys. J.* **2006**; *647*, 1535.
[8] S. G. Buckley, C. J. Damm, W. M. Vitovec, L. A. Sgro, R. F. Sawyer, C. P. Koshland, D. Lucas, *Appl. Opt.* **1998**; *37*, 8382.
[9] U. Westblom, M. Aldén, *Appl. Spectrosc.* **1990**; *44*, 881.
[10] C. Brackmann, O. Hole, B. Zhou, Z. S. Li, M. Aldén, *Appl. Phys. B: Lasers Opt.* **2014**; *115*, 25.
[11] K. Nyholm, R. Fritzon, N. Georgiev, M. Aldén, *Opt. Commun.* **1995**; *114*, 76.
[12] N. Georgiev, M. Aldén, *Appl. Phys. B: Photophys. Laser Chem.* **1993**; *56*, 281.
[13] M. N. R. Ashfold, D. W. Chandler, C. C. Hayden, R. I. McKay, A. J. R. Heck, *Chem. Phys.* **1995**; *201*, 237.
[14] W. Meienburg, H. Neckel, J. Wolfrum, *Appl. Phys. B: Photophys. Laser Chem.* **1990**; *51*, 94.
[15] A. P. Force, D. K. Killinger, W. E. DeFeo, N. Menyuk, *Appl. Opt.* **1985**; *24*, 2837.
[16] R. Claps, F. V. Englich, D. P. Leleux, D. Richter, F. K. Tittel, R. F. Curl, *Appl. Opt.* **2001**; *40*, 4387.
[17] A. Goldman, I. Rahinov, S. Cheskis, B. Löhden, S. Wexler, K. Sengstock, V. M. Baev, *Chem. Phys. Lett.* **2006**; *423*, 147.
[18] M. Gutfleisch, D. I. Shin, T. Dreier, P. M. Danehy, *Appl. Phys. B: Lasers Opt.* **2000**; *71*, 673.
[19] P. Ewart, S. V. O'Leary, *Opt. Lett.* **1986**; *11*, 279.
[20] P. Ewart, P. Snowdon, *Opt. Lett.* **1990**; *15*, 1403.
[21] R. L. Farrow, D. J. Rakestraw, *Science* **1992**; *257*, 1894.
[22] R. L. Abrams, R. C. Lind, *Opt. Lett.* **1978**; *2*, 94.
[23] R. L. Abrams, R. C. Lind, *Opt. Lett.* **1978**; *3*, 205.
[24] B. Attal-Trétout, H. Bervas, J. P. Taran, S. L. Boiteux, P. Kelley, T. K. Gustafson, *J. Phys. B: At. Mol. Opt. Phys.* **1997**; *30*, 497.
[25] T. A. Reichardt, W. C. Giancola, C. M. Shappert, R. P. Lucht, *Appl. Opt.* **1999**; *38*, 6951.
[26] J. Kiefer, P. Ewart, *Prog. Energy Combust. Sci.* **2011**; *37*, 525.
[27] R. L. Vander Wal, B. E. Holmes, J. B. Jeffries, P. M. Danehy, R. L. Farrow, D. J. Rakestraw, *Chem. Phys. Lett.* **1992**; *191*, 251.
[28] G. J. Germann, D. J. Rakestraw, *Science* **1994**; *264*, 1750.
[29] Y. Tang, S. A. Reid, *Chem. Phys. Lett.* **1996**; *248*, 476.
[30] G. J. Germann, R. L. Farrow, D. J. Rakestraw, *J. Opt. Soc. Am. B* **1995**; *12*, 25.
[31] Z. W. Sun, Z. S. Li, B. Li, M. Aldén, P. Ewart, *Appl. Phys. B: Lasers Opt.* **2010**; *98*, 593.
[32] Z. W. Sun, Z. S. Li, B. Li, M. Aldén, *J. Raman Spectrosc.* **2011**; *42*, 1828.
[33] A. L. Sahlberg, J. Zhou, M. Aldén, Z. S. Li, *J. Raman Spectrosc.* **2015**; *46*, 695.
[34] L. Høgstedt, J. S. Dam, A.-L. Sahlberg, Z. Li, M. Aldén, C. Pedersen, P. Tidemand-Lichtenberg, *Opt. Lett.* **2014**; *39*, 5321.

[35] Z. S. Li, C. H. Hu, J. Zetterberg, M. Linvin, M. Alden, *J. Chem. Phys.* **2007**; *127*, 084310.
[36] Z. S. Li, M. Rupinski, J. Zetterberg, Z. T. Alwahabi, M. Aldén, *Chem. Phys. Lett.* **2005**; *407*, 243.
[37] L. S. Rothman, I. E. Gordon, Y. Babikov, A. Barbe, D. Chris Benner, P. F. Bernath, M. Birk, L. Bizzocchi, V. Boudon, L. R. Brown, A. Campargue, K. Chance, E. A. Cohen, L. H. Coudert, V. M. Devi, B. J. Drouin, A. Fayt, J.-M. Flaud, R. R. Gamache, J. J. Harrison, J. M. Hartmann, C. Hill, J. T. Hodges, D. Jacquemart, A. Jolly, J. Lamouroux, R. J. Le Roy, G. Li, D. A. Long, O. M. Lyulin, C. J. Mackie, S. T. Massie, S. Mikhailenko, H. S. P. Müller, O. V. Naumenko, A. V. Nikitin, J. Orphal, V. Perevalov, A. Perrin, E. R. Polovtseva, C. Richard, M. A. H. Smith, E. Starikova, K. Sung, S. Tashkun, J. Tennyson, G. C. Toon, V. G. Tyuterev, G. Wagner, *J. Quant. Spectrosc. Radiat. Transfer.* **2013**; *130*, 4.
[38] L. S. Rothman, I. E. Gordon, R. J. Barber, H. Dothe, R. R. Gamache, A. Goldman, V. I. Perevalov, S. A. Tashkun, J. Tennyson, *J. Quant. Spectrosc. Radiat. Transfer* **2010**; *111*, 2139.
[39] H. Bervas, S. L. Boiteux, B. Attal-Trétout, J. P. Taran, *J. Phys. B: At. Mol. Opt. Phys.* **1992**; *25*, 949.
[40] J. Cooper, A. Charlton, D. R. Meacher, P. Ewart, G. Alber, *Phys. Rev. A.* **1989**; *40*, 5705.
[41] W. S. Benedict, E. K. Plyler, E. D. Tidwell, *J. Res. Natl. Bur. Stand.* **1958**; *61*, 123.
[42] M. J. Down, C. Hill, S. N. Yurchenko, J. Tennyson, L. R. Brown, I. Kleiner, *J. Quant. Spectrosc. Radiat. Transfer* **2013**; *130*, 260.
[43] L. S. Rothman, I. E. Gordon, A. Barbe, D. C. Benner, P. F. Bernath, M. Birk, V. Boudon, L. R. Brown, A. Campargue, J.-P. Champion, K. Chance, L. H. Coudert, V. Dana, V. M. Devi, S. Fally, J.-M. Flaud, R. R. Gamache, A. Goldman, D. Jacquemart, I. Kleiner, N. Lacome, W. J. Lafferty, J.-Y. Mandin, S. T. Massie, S. N. Mikhailenko, C. E. Miller, N. Moazzen-Ahmadi, O. V. Naumenko, A. V. Nikitin, J. Orphal, V. I. Perevalov, A. Perrin, A. Predoi-Cross, C. P. Rinsland, M. Rotger, M. Šimečková, M. A. H. Smith, K. Sung, S. A. Tashkun, J. Tennyson, R. A. Toth, A. C. Vandaele, J. Vander Auwera, *J. Quant. Spectrosc. Radiat. Transfer* **2009**; *110*, 533.
[44] Š. Urban, N. Tu, K. Narahari Rao, G. Guelachvili, *J. Mol. Spectrosc.* **1989**; *133*, 312.
[45] K. Bultitude, R. Bratfalean, P. Ewart, *J. Raman Spectrosc.* **2003**; *34*, 1030.
[46] T. A. Reichardt, R. P. Lucht, *J. Opt. Soc. Am. B* **1997**; *14*, 2449.
[47] G. M. Lloyd, P. Ewart, *J. Chem. Phys.* **1999**; *110*, 385.
[48] W. D. Monnery, K. A. Hawboldt, A. E. Pollock, W. Y. Svrcek, *Ind. Eng. Chem. Res.* **2001**; *40*, 144.
[49] I. Rahinov, N. Ditzian, A. Goldman, S. Cheskis, *Appl. Phys. B: Lasers Opt.* **2003**; *77*, 541.
[50] T. Dreier, D. J. Rakestraw, *Opt. Lett.* **1990**; *15*, 72.
[51] T. A. Reichardt, R. P. Lucht, *J. Opt. Soc. Am. B* **1996**; *13*, 1107.
[52] P. M. Danehy, E. J. Friedmanhill, R. P. Lucht, R. L. Farrow, *Appl. Phys. B: Photophys. Laser Chem.* **1993**; *57*, 243.
[53] D.-H. Yu, J.-H. Lee, J.-S. Chang, J. W. Hahn, *J. Opt. Soc. Am. B* **1999**; *16*, 1261.
[54] R. L. Farrow, D. J. Rakestraw, T. Dreier, *J. Opt. Soc. Am. B* **1992**; *9*, 1770.
[55] J. S. Dam, P. Tidemand-Lichtenberg, C. Pedersen, *Nat. Photonics* **2012**; *6*, 788.
[56] W. Torres, S. S. Pansare, J. G. Goodwin, *Catal. Rev.: Sci. Eng.* **2007**; *49*, 407.
[57] W. de Jong, A. Pirone, M. A. Wójtowicz, *Fuel* **2003**; *82*, 1139.